JAAS

Accepted Manuscript

This is an *Accepted Manuscript*, which has been through the Royal Society of Chemistry peer review process and has been accepted for publication.

Accepted Manuscripts are published online shortly after acceptance, before technical editing, formatting and proof reading. Using this free service, authors can make their results available to the community, in citable form, before we publish the edited article. We will replace this *Accepted Manuscript* with the edited and formatted *Advance Article* as soon as it is available.

You can find more information about *Accepted Manuscripts* in the Information for Authors.

Please note that technical editing may introduce minor changes to the text and/or graphics, which may alter content. The journal's standard Terms & Conditions and the Ethical guidelines still apply. In no event shall the Royal Society of Chemistry be held responsible for any errors or omissions in this *Accepted Manuscript* or any consequences arising from the use of any information it contains.

ROYAL SOCIETY OF CHEMISTRY

www.rsc.org/jaas

Cite this: DOI: 10.1039/c0xx00000x

www.rsc.org/xxxxxx

ARTICLE TYPE

Sensitivity improvement in detection of V and Mn elements in steel using laser-induced breakdown spectroscopy with ring-magnet confinement

Zhongqi Hao, Lianbo Guo, Changmao Li, Meng Shen, Xiaoheng Zou, Xiangyou Li,* Yongfeng Lu and Xiaoyan Zeng

Received (in XXX, XXX) XthXXXXXXXXX 20XX, Accepted Xth XXXXXXXXX 20XX
DOI: 10.1039/b000000x

To improve the detection sensitivity of vanadium (V) and manganese (Mn) elements in steel using laser-induced breakdown spectroscopy (LIBS), a ring magnet was used to spatially and magnetically confine plasmas produced from steel samples using an Nd:YAG laser. The results showed that the optical emission and signal-to-noise ratios (SNRs) for both V I 437.92 nm and Mn I 403.08 nm lines were enhanced with ring-magnet confinement. The enhancements were found to be due to an increase in the plasma temperature and electron density as a result of both spatial and magnetic confinement. The calibration curves of V I 437.92 nm and Mn I 403.08 nm with/without confinement were established. The 3σ-limits of detection (LoDs) for V and Mn in steels were 11 and 30 ppm with the ring magnet, lower than the 18 and 41 ppm with a degaussed magnet, and the 41 and 56 ppm in open air.

1. Introduction

Laser-induced breakdown spectroscopy (LIBS) has become a popular analytical technique during past decades[1] due to its unique features, including applicability to any type of sample, no or simple sample preparation, nearly nondestructive, simultaneous multi-element detection, standoff sensing capability, and rapid in situ analysis.[2-4] Due to these advantages, LIBS has a wide range of potential applications in fields such as environmental science, biotechnology, industry, agriculture, forensics, combustion, and defense.[5-8]

Currently, one problem with LIBS is its low sensitivity in determining trace elements. Several methods have been proposed to improve LIBS sensitivity, such as double-pulse (DP),[9] multi-pulse (MP),[10, 11] Nanoparticle-enhanced LIBS (NELIBS),[12] spatial confinement, and magnetic confinement. Among these methods, spatial confinement is simple and cost-effective for enhancing signal strength and improving the detection sensitivity of LIBS.

X.Z. Zeng *et al.*[13] studied the formation of laser-induced plasmas inside a series of truncated cones. The cavity effects on plasma expansion were investigated. X.K. Shen *et al.*[14] used a cylindrical pipe to confine aluminum plasmas. A maximal enhancement factor of 9 was obtained at a pipe diameter of 10.8 mm. A.M. Popov *et al.*[15, 16] used a small chamber to confine iron and soil plasmas with enhancement factors of 3 and 10 for arsenic (As) and iron (Fe) signals, and the limits of detection (LoDs) of trace elements in soil were 2–5 times better than those detected using free-expanding plasmas. P. Yeates *et al.*[17] investigated the variation of spectroscopic, imaging, and probe diagnostics of laser plasma plumes within rectangular cavities of fixed depth and varying height. Z. Wang *et al.*[18, 19] adopted a cylindrical cavity of 1.5 mm in height and 3 mm in diameter to confine coal plasmas and reported enhanced emission intensity with reduced shot-to-shot fluctuation. In addition, several previous works in our research group reported enhancement effects[20, 21] with accuracy improvement[22] of quantitative analysis using a series of hemispheric cavities to confine laser-induced plasmas. Furthermore, a few studies reported the magnetic field confinement effects in LIBS. S.S. Harilal *et al.*[23] reported the confinement and dynamics of laser-produced plasma expansion across a 0.64 T magnetic field. The electron density and temperature in LIBS plasmas were observed to increase because of higher collision frequency in the presence of the magnetic field. X.K. Shen *et al.*[24] used a magnetic field of ~0.8 T to confine plasmas from aluminum (Al) and copper (Cu) targets, with enhancement factors of 2 and 6–8 for Al and Cu lines. N.R. Virendra *et al.*[25] investigated the enhancement of LIBS signals of solid and liquid samples under a ~0.5 T magnetic field. The enhancement factors could reach 2 and 1.5 for solid and liquid samples, respectively.

From the discussion above, we can understand that both spatial and magnetic confinements are effective in LIBS signal enhancement. To combine the advantages of spatial and magnetic confinements, Guo *et al.*[26] used a pair of permanent magnets and a hemispherical cavity simultaneously to confine plasmas produced from metal samples using a KrF Excimer laser. Enhancement factors of about 22 and 24 were obtained in emission intensity of the cobalt (Co) and chromium (Cr) lines. Nevertheless, this research focused mainly on the enhancement of optical emissions rather than signal-to-noise ratios (SNRs), which represent the sensitivity of LIBS. Additionally, the quantitative

analysis and the LoD were not investigated in that work.

The aim of this study was to investigate the improvement of detection sensitivity of vanadium (V) and manganese (Mn) elements in steels using LIBS with ring-magnet confinement, which combines spatial and magnetic confinements of laser-induced plasmas. The experimental results confirmed that the optical emission intensity, SNR, and LoD of LIBS all improved with ring-magnet confinement.

2. Experimental methods

The schematic diagram of the experimental setup used in this work is shown in Fig.1. A Q-switched Nd:YAG laser (Quantel Brilliant B, maximum energy: 400 mJ/pulse, wavelength: 532 nm, pulse width: 5 ns) was used for plasma generation. The laser beam was reflected by a dichroic mirror (reflection band: about 474-554 nm) and focused by a convex lens (focal length: 20 cm) through the hole of the ring magnet onto the steel target. The optical emission from the laser-induced plasmas was collected by an optical fiber through another UV-grade quartz lens placed on top of the dichroic mirror, and the fiber was coupled into an echelle spectrometer (Andor Tech., Mechelle 5000, 200-950 nm, spectral resolution: $\lambda/\Delta\lambda$ = 5000). The spectrally resolved lines were detected by a 1024×1024 pixel intensified charge coupled device (ICCD) (Andor Tech., iStar DH-334T). Both the laser and ICCD were synchronized by a digital delay generator (Stanford Research System DG535, delay resolution: 5 ps). Data acquisition and analysis were performed with a personal computer. In this study, each spectrum was averaged by ten different locations on a sample under the same experimental conditions.

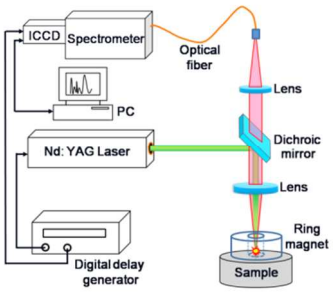

Fig. 1 Schematic diagram of the experimental setup.

The magnetic field intensity (B) distribution of the NdFeB ring magnet that was placed on the steel sample is given in Fig. 2, and the inset shows the structure of the ring magnet used in the experiment. Its outer diameter (D), inner diameter (d), and height (H) were 12.7, 3.2, and 6.3 mm, respectively. The axial line of the magnet and its intersection with the sample surface were defined as the X-axis and origin O (x = 0). As shown in Fig. 2, the magnetic field of the ring magnet (circle dots) increased gradually along the X-axis. The initial magnetic field was 3080 G at the origin O; and then the value reached a maximum of about 4090 G at 3.2 mm, corresponding to the half-height position of the ring magnet. The magnetic field then decreased rapidly as the distance increased and reduced to 0 near the exit of the cavity. To confirm the effect of magnetic confinement, the same magnet was degaussed by heat treatment at 500 ℃ for 10 min. The magnetic field of the degaussed magnet (square dots) decreased to ~0 G, so the degaussed magnet only had the spatial confinement effects for plasma plumes.

Seven steel samples (GSB03-2582-2010, Pangang Group Research Institute Co. Ltd, China,) were used in this work. The concentrations of V and Mn are listed in Table 1.

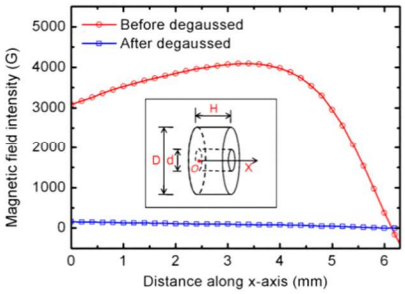

Fig. 2 Magnetic field intensity before (circle dots) and after (square dots) degaussing along the X-axis of the ring magnet (inset: magnet structure: D = 12.7 mm, d = 3.2 mm, H = 6.3 mm).

Table 1. Compositions of V and Mn in Steel Samples

No.	V (% wt)	Mn (% wt)
1	0.009	0.072
2	0.044	0.0329
3	0.071	1.22
4	0.158	0.857
5	0.335	0.596
6	0.506	1.46
7	0.821	2.06

3. Results and discussion

3.1 Optical emission enhancement and physical mechanisms

The time-integrated LIBS spectra from sample No. 7 were measured with a time delay of 2 μs after the laser pulse and a gate width of 0.5 μs. The focal point of the lens was 4 mm under the sample surface to avoid air breakdown. The laser energy was 60 mJ/pulse. The spectra presented here were averaged over 20 laser pulses to reduce the intensity deviation. Figure 3 shows the representative spectra of steel sample No. 7 in the range between 402.5 nm and 440 nm with the ring magnet (solid curve), with the degaussed magnet (dashed curve), and without confinement (dotted curve). Obviously, the emission intensities of Mn and V were enhanced with both the magnet and degaussed magnet confinements. Furthermore, the enhancement effect with the ring magnet was greater than that with the degaussed magnet.

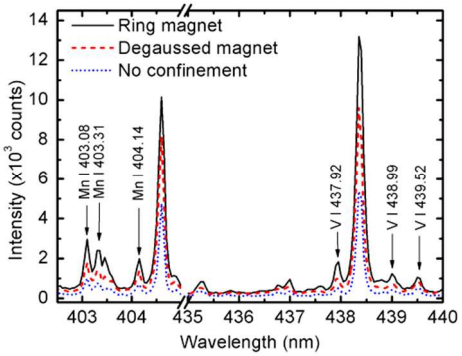

Fig. 3 Time-integrated spectra from steel sample No. 7 with ring magnet (solid curve), with degaussed magnet (dashed curve), and without confinement (dotted curve).

Figure 4 depicts the temporal evolution of the emission intensities from (a) V I (437.92 nm) and (b) Mn I (403.08 nm) peaks as functions of the gate delay with the ring magnet, with the degaussed magnet, and without confinement. The error bars may come from the pulse-to-pulse energy fluctuation and the deviation of the magnet position among different measurements. It can be seen that the intensity enhancement was different with different delay times, from about 1 to 6 μs. During this time period, there were two times the intensity enhancement effects at time delays of 2 μs and 4.5 μs for confinement both with a ring magnet and with a degaussed magnet. Maximum enhancement factors of 3.1 and 2.8 with the ring magnet for V I 437.92 nm and Mn I 403.08 nm were obtained at a time delay of 2 μs, while the enhancement factors were only about 2.7 and 2.3 with the degaussed magnet at the same time delay.

It is clear that stronger enhancements were observed before the ring magnet was degaussed, which indicates that laser-induced plasmas were under both spatial and magnetic confinements. A shock wave is produced by the initial explosive pressure along with the plasma generation and supersonic expansion.[27] When the shock wave encounters the cavity wall, it is reflected and travels back towards the plasma. If the cavity is small and the shockwave energy is sufficiently large, multiple reflections can occur, corresponding to multiple enhanced peaks in the emissive intensity. Shen and Popov et al.[14, 15] have observed the phenomenon of twice enhanced peaks by spatially confining the laser-induced plasma, and the latter peaks appear at a longer delay times owing to the velocity decaying of the shock wave.[28] Similarly, as shown in Fig. 4, the two enhanced peaks appeared at 2 and 4.5 μs. When an external magnetic field is applied on the plasma, the movement of electrons and ions in the plasmas are affected by the Lorentz force. The plasma expansion is decelerated, and the size of the plume is reduced. This may lead to the increase in effective electron density in the plume and result in the enhancement of optical emission. The enhancement of the plasma emission under the influence of a magnetic field can be given as:[25]

$$\frac{I_2}{I_1}=\left(1-\frac{1}{\beta}\right)^{-3/2}\left(\frac{t_1}{t_2}\right)^3 . \quad (1)$$

Eq. (1) indicates that the intensity enhancement (I_2/I_1) of plasma emission in the presence of a magnetic field depends on the plasma parameter β as well as the ratio of the duration of the emission (t_1/t_2). At the same delay time and gate width, $t_1 = t_2$.The plasma parameter β is the ratio of kinetic energy of plasma to the magnetic energy, and it can be expressed as:

$$\beta=\frac{8\pi n_e kT_e}{B^2}, \quad (2)$$

where n_e is the electron density (cm^{-3}), k is the Boltzmann constant, T_e is the electron temperature (eV), and B is the magnetic field (G).

According to Eq. (1) and (2), the emission enhancement becomes possible only when β is sufficiently small, which requires a stronger B, lower T_e or lower n_e.[23-26] For this reason, no enhancement occurs for initial hot plasma when the delay time is smaller. When the magnet is degaussed, $B = 0$ and β tends to be infinity, thus $I_2/I_1 = 1$, namely the effect of magnetic confinement to plasma disappears, which explains why the intensity enhancement factors became lower after the magnet is degaussed.

To further understand the intensity enhancement effects due to spatial and magnetic confinement, the variations of T_e and n_e at different delay times were studied.

In this work, T_e was estimated base on Boltzmann plot using iron atomic lines.[29] As shown in Fig. 5, T_e is about 12,000 K at delay time of 0.5 μs without any confinement, and then T_e started to decrease quickly. Comparably, the values of T_e with ring magnet were highest and those with the degaussed magnet were moderate at the delay times from 1 to 6 μs. The reason may due to the magnetic and spatial confinement.

The electron densities with/without confinement were evaluated from width of H_α following the formula:[30]

$$N_e(H_\alpha)=8.02\times10^{12}\left(\Delta\lambda_{1/2}/\alpha_{1/2}\right)^{3/2} cm^{-3}, \quad (3)$$

where $\Delta\lambda_{1/2}$ is the full width at half maximum (FWHM) of the

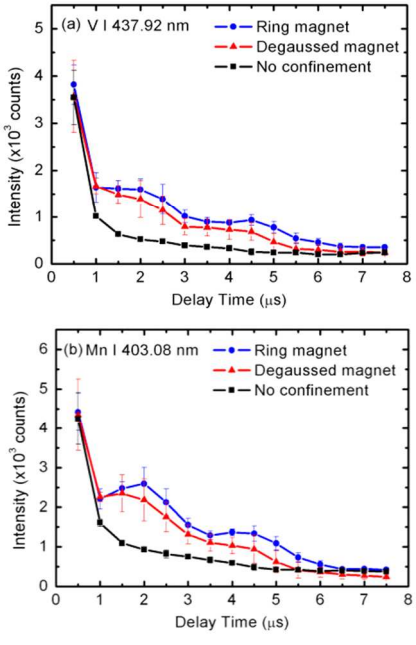

Fig. 4 Emission intensities of V I 437.92 nm (a) and Mn I 403.08 nm (b) at different delay times with a ring magnet (circle dots), with a degaussed magnet (triangle dots), and without confinement (square dots).Gate width: 0.5 μs.

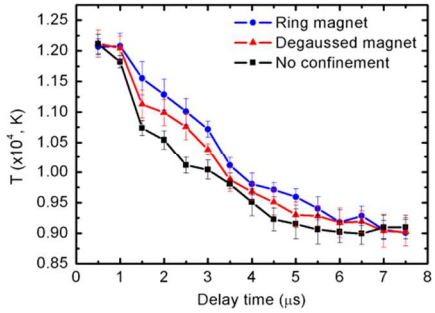

Fig. 5 Variation of the electron temperature at different delay times with a ring magnet (circle dots), with a degaussed magnet (triangle dots), and without confinement (square dots). Gate width: 0.5 μs.

H_α-lines, $\alpha_{1/2}$ is the half width of the reduced Stark profiles.[31] The temporal variations of the n_e were shown in Fig. 6. The values of n_e without confinement are about 6×10^{17} cm^{-3} at delay time of 0.5 μs, then the n_e decreased rapidly with the delay times. The n_e with the degaussed magnet were higher than the values without confinement at delay times from 1 to 6 μs owing to the spatial confinement effect, and the n_e with the ring magnet were highest due to the spatial and magnetic confinement simultaneously.

Furthermore, the values of T_e, n_e and B with the ring magnet were substituted into Eq. (2) to calculate the values of β. At a certain delay time, the T_e and n_e are constant, but the B is varied along with X-axis. Therefore, the variation of β with X can be obtained. After that, the values of I_2/I_1 with X were acquired by substituting β into Eq. (1).

The variations of β and I_2/I_1 along the X-axis at different delay times (0.5, 2, 3.5, and 4.5 μs) were shown in Fig. 7 (a) and (b), respectively. As Fig. 7 (a) shows, along with X-axis, the values of β begin to decrease gradually, and then increased sharply. The minimum appeared at X=3.2 mm, corresponding to the position of the maximum magnetic field. Comparing the curves at different delay times, the values of β decreased with the increasing of the delay times due to the decreasing of T_e and n_e.

In Fig. 7 (b), the I_2/I_1 increase continuously along with X-axis until reached a peak at X of 3.2 mm, and then the I_2/I_1 rapidly decreased. The values of I_2/I_1>1, that means the magnetic field can cause the emission enhancement. For the curves with decreasing delay times, the I_2/I_1 became smaller. Therefore, at the delay time of 0.5 μs, the enhancement effect was very weak.

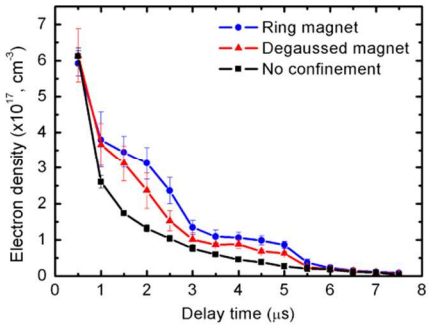

Fig. 6 Variation of the electron density at different delay times with a ring magnet (circle dots), with a degaussed magnet (triangle dots), and without confinement (square dots). Gate width: 0.5 μs.

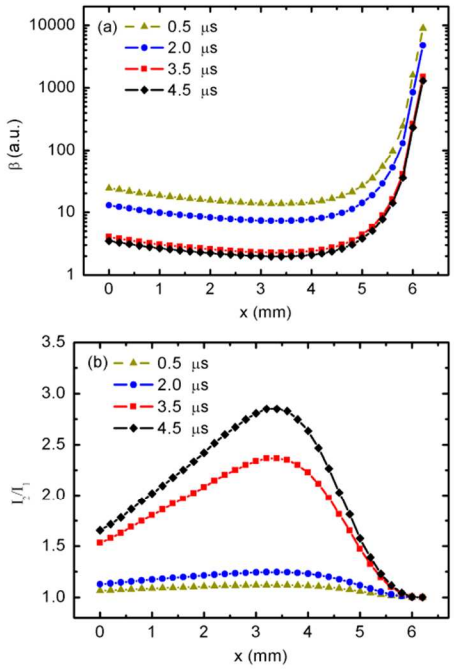

Fig. 7 Variation of β (a) and I_2/I_1 (b) along with X-axis of the ring magnet at delay times of 0.5 (triangle dots), 2 (circle dots), 3.5 (square dots), and 4.5 μs (diamond dots).

3.2 Enhancement of signal-to-noise ratios (SNR）

A substantial amount of effort was devoted to increasing the spectral SNR, as larger SNRs result in lower LoDs. The SNR is defined as the ratio of the spectral intensity to the standard deviation of the background. The spectral range from 436.09 to 436.40 nm was selected as the blank background in this work. Figure 8 illustrates the SNRs of V I 437.92 nm (a) and Mn I 403.08 nm (b) with a ring magnet, with a degaussed magnet, and without confinement, respectively. As shown in Fig. 8, the SNR reached maximum at a time delay of 2.5 μs but not 2 μs, corresponding to the maximum intensity enhancement factors in Fig. 4 (a) and (b). This is because the decay of the noise is faster than the signal under confinement. At the beginning, n_e and T_e increase sharply because of the compression of the reflected shock wave. The noise is enhanced during this fast variation of plasma conditions. After the energy of the shock wave is consumed, the noise decreases quickly due to the compressed plasma expanding relatively smoothly, but the optical emission of excited atomic decays slowly with the decrease in n_e and T_e in expanding plasma plumes.

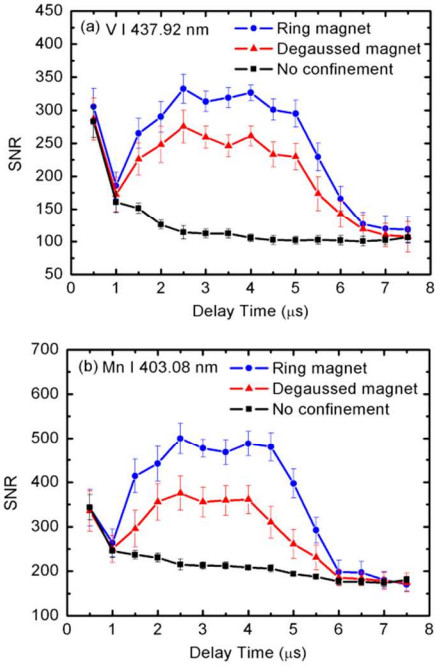

Fig. 8 Signal-to-noise ratios of V I 437.92 nm (a) and Mn I 403.08 nm (b) with a ring magnet (circle dots), with a degaussed magnet (triangle dots), and without confinement (square dots).

SNR enhancement factors of about 2.9 and 2.3 were achieved at 2.5 μs for V I 437.92 nm and Mn I 403.08 nm with the ring magnet, while only 2.4 and 1.7 were acquired with the degaussed magnet, respectively. This suggested that the confinement with the ring magnet was more effective than the nonmagnetic ring cavity in improving LIBS sensitivity (SNR).

3.3 Quantitative analysis and limit of detection

The discussion above reveals that the enhancement of emission intensity and SNR appeared during the delay times from 1 to 6 μs. Therefore, in the quantitative analyses and LoDs estimation for V and Mn, the delay time and the gate width were fixed to 1 and 5 μs, respectively. The calibration curves of seven reference steel samples for V I 437.92 nm and Mn I 403.08 nm in three cases are shown in Fig. 9. To estimate LoDs of V and Mn in the steels, the well-known 3σ-criterion was used in the following formulae:

$$LoD = 3\sigma_B / S, \quad (4)$$

where σ_B is the standard deviation of the background, and S is the slope of the calibration curve. As seen in Fig. 9 (a) and (b), the slopes of the calibration curves with the ring magnet, the degaussed magnet, and no confinment decreased gradually. The LoDs of V were 11, 18, and 41 ppm when a ring magnet, a degaussed ring magnet, and no confinement were used, respectively. The corresponding LoDs of Mn were 30, 41, and 56 ppm, respectively. Obviously, the sensitivity can be further improved using ring-magnet confinement rather than a nonmagnetic ring. In addition, the intercepts of the calibration curves were almost unchanged before and after the magnet was degaussed for both elements, presumably because the magnetic field enhanced the optical emission but had no effect on the bremsstrahlung radiation.[25] Hence, the continuous background was almost unchanged in the presence of the magnetic field.

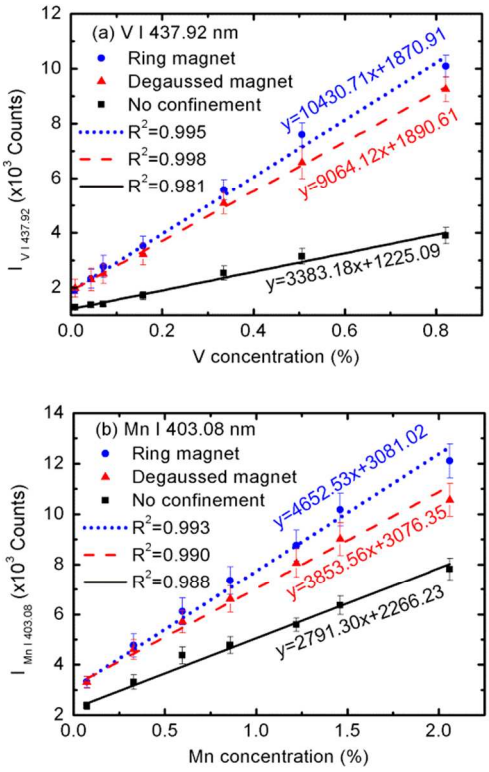

Fig. 9 Calibration curves of (a) V and (b) Mn in the referenced steel samples with a ring magnet (circle dots), with a degaussed magnet (triangle dots), and without confinement (square dots).

It should be noted that when the LoDs were reduced, the accuracy of the quantitative analyses with the magnetic and nonmagnetic ring confinements showed improvement rather than deterioration. As shown in Fig. 9, the determination coefficients (R^2) of the calibration curves for V I 437.92 nm and Mn I 403.08 nm with the ring-magnet confinement were larger than those without confinement. The reason might be that the compressed plasma plumes became more uniform under the spatial and magnetic confinements than those in open air.

4. Conclusions

In summary, the sensitivity improvement of V and Mn in steels using LIBS combined with ring-magnet confinement was investigated by optical emission intensity, SNR, and LoD. The intensity enhancement effect with a ring magnet is attributed to the simultaneous spatial and magnetic confinement, which can increase the temperature and electron density of the plasma. The SNR enhancement factors of about 2.9 and 2.3 were obtained at a time delay of 2.5 μs for the V I 437.92 nm and Mn I 403.08 nm lines with the ring magnet and 2.4 and 1.7 with the degaussed magnet. The calibration curves of V I 437.92 nm and Mn I 403.08 nm were given with a ring magnet, with a degaussed magnet, and without confinement. Finally, the quantitative analyses curves of V I 437.92 nm and Mn I 403.08 nm elements with/without confinement were established. The LoDs of V and Mn were estimated using 3σ-criterion. The results showed that with ring-magnet confinement, the LoDs of V and Mn in steels decreased to 11 and 30 ppm, lower than the 18 and 41 ppm with a degaussed magnet, and the 41 and 56 ppm with no confinement.

Acknowledgement

This research was financially supported by the Major Scientific Instruments and Equipment Development Project of China (No. 2011YQ160017), by the National Natural Science Foundation of China (No. 51128501), and by the China Postdoctoral Science Foundation (No. 2013M542014).

Notes and References

Wuhan National Laboratory for Optoelectronics (WNLO), Huazhong University of Science and Technology, Wuhan, Hubei 430074, PR China. Fax: 86-27-87541423; Tel: 86-27-87541423; E-mail: xyli@mail.hust.edu.cn

1. C. Pasquini, J. Cortez, L. M. C. Silva and F. B. Gonzaga, *Journal of the Brazilian Chemical Society*, 2007, **18**, 463-512.
2. D. W. Hahn and N. Omenetto, *Appl. Spectrosc.*, 2010, **64**, 335A-366A.
3. F. C. DeLucia Jr, A. C. Samuels, R. S. Harmon, R. A. Walters, K. L. McNesby, A. Lapointe, R. J. Winkel Jr and A. W. Miziolek, *Sensors Journal, IEEE*, 2005, **5**, 681-689.
4. R. S. Harmon, F. C. DeLucia, C. E. McManus, N. J. McMillan, T. F. Jenkins, M. E. Walsh and A. Miziolek, *Applied geochemistry*, 2006, **21**, 730-747.
5. A. K. Knight, N. L. Scherbarth, D. A. Cremers and M. J. Ferris, *Appl. Spectrosc.*, 2000, **54**, 331-340.
6. D. W. Hahn and N. Omenetto, *Appl. Spectrosc.*, 2012, **66**, 347-419.

7. L. Radziemski and D. Cremers, *Spectrochimica Acta Part B: Atomic Spectroscopy*, 2013, **87**, 3-10.
8. Z. Wang, T.-B. Yuan, Z.-Y. Hou, W.-D. Zhou, J.-D. Lu, H.-B. Ding and X.-Y. Zeng, *Frontiers of Physics*, 2014, 1-19.
9. V. Babushok, F. DeLucia Jr, J. Gottfried, C. Munson and A. Miziolek, *Spectrochimica Acta Part B: Atomic Spectroscopy*, 2006, **61**, 999-1014.
10. G. Galbacs, N. Jedlinszki, K. Herrera, N. Omenetto, B. Smith and J. Winefordner, *Appl. Spectrosc.*, 2010, **64**, 161-172.
11. N. Jedlinszki and G. Galbács, *Microchemical Journal*, 2011, **97**, 255-263.
12. A. De Giacomo, R. Gaudiuso, C. Koral, M. Dell'Aglio and O. De Pascale, *Analytical chemistry*, 2013, **85**, 10180-10187.
13. X. Zeng, S. S. Mao, C. Liu, X. Mao, R. Greif and R. E. Russo, *Spectrochimica Acta Part B: Atomic Spectroscopy*, 2003, **58**, 867-877.
14. X. Shen, J. Sun, H. Ling and Y. Lu, *Journal of applied physics*, 2007, **102**, 093301.
15. A. M. Popov, F. Colao and R. Fantoni, *Journal of Analytical Atomic Spectrometry*, 2009, **24**, 602-604.
16. A. M. Popov, F. Colao and R. Fantoni, *Journal of Analytical Atomic Spectrometry*, 2010, **25**, 837-848.
17. P. Yeates and E. Kennedy, *Journal of Applied Physics*, 2010, **108**, 093306.
18. Z. Wang, Z. Hou, S.-l. Lui, D. Jiang, J. Liu and Z. Li, *Optics express*, 2012, **20**, A1011-A1018.
19. Z. Hou, Z. Wang, J. Liu, W. Ni and Z. Li, *Optics express*, 2013, **21**, 15974-15979.
20. L. Guo, C. Li, W. Hu, Y. Zhou, B. Zhang, Z. Cai, X. Zeng and Y. Lu, *Applied Physics Letters*, 2011, **98**, 131501.
21. C. Li, Y.-F. Lu, L. Guo, X. Li, X. Zeng, X. N. He and Z. Hao, *Journal of Analytical Atomic Spectrometry*, 2014.
22. L. Guo, Z. Hao, M. Shen, W. Xiong, X. He, Z. Xie, M. Gao, X. Li, X. Zeng and Y. Lu, *Optics express*, 2013, **21**, 18188-18195.
23. S. Harilal, M. Tillack, B. O'shay, C. Bindhu and F. Najmabadi, *Physical Review E*, 2004, **69**, 026413.
24. X. Shen, Y. Lu, T. Gebre, H. Ling and Y. Han, *Journal of applied physics*, 2006, **100**, 053303.
25. V. N. Rai, A. K. Rai, F.-Y. Yueh and J. P. Singh, *Applied optics*, 2003, **42**, 2085-2093.
26. L. Guo, W. Hu, B. Zhang, X. He, C. Li, Y. Zhou, Z. Cai, X. Zeng and Y. Lu, *Optics express*, 2011, **19**, 14067-14075.
27. D. Bivolaru and S. Kuo, *Physics of Plasmas* 2002, **9**, 721-723.
28. Y. Qian, J. Lu and X. Ni, *Chinese Optics Letters*, 2009, **7**, 410-412.
29. R. Noll, *Laser-Induced Breakdown Spectroscopy*, Springer. 2012.
30. J. Ashkenazy, R. Kipper and M. Caner, *Physical Review A*, 1991, **43**, 5568.
31. H. Griem, *Academic, New York*, 1997.